Materials Today Chemistry 48 (2025) 103022

Contents lists available at ScienceDirect

Materials Today Chemistry

journal homepage: www.journals.elsevier.com/materials-today-chemistry/

UV-light assisted hybrid InSe-graphene gas sensor for the detection of NO_2

Jyayasi Sharma [a,b,c], Frank Güell [a,d], Mubdiul Islam Rizu [a,b,c], Dalal Fadil [a,b,c], Eduard Llobet [a,b,c,*]

[a] Universitat Rovira i Virgili, MINOS, School of Engineering, Avda. Països Catalans 26, 43007, Tarragona, Spain
[b] IU-RESCAT, Research Institute in Sustainability, Climatic Change and Energy Transition, Universitat Rovira i Virgili, Joanot Martorell 15, 43480, Vila-seca, Spain
[c] TecnATox - Centre for Environmental, Food and Toxicological Technology, Universitat Rovira i Virgili, Avda. Països Catalans 26, 43007, Tarragona, Spain
[d] Universitat de Barcelona, Catalan Photonics for Energy (ENFOCAT), Barcelona, Catalunya, Spain

ARTICLE INFO

Keywords:
Liquid phase exfoliation (LPE)
UV excitation
Gas sensor
hybrid InSe/graphene

ABSTRACT

This work presents a novel light-modulated gas sensor based on hybrid Indium Selenide (InSe)-graphene synthesized via the liquid phase exfoliation (LPE) technique. We investigated the effects of the operating temperature and light irradiation on the sensing layer performance. The morphology, composition and structural characteristics of the sensing layer are analyzed using different material characterization techniques including scanning and transmission electron microscopies, X-ray photoelectron spectroscopy, and Raman. The response to $^{NO}_{2}$ of the InSe-graphene hybrid gas sensor while operated under dark conditions or excited at one of three different wavelengths (i.e., 375, 470, and 530 nm), which correspond to UV, blue and green light, respectively, is studied. Results show that UV light excitation of the film when operated either at room temperature or at 150 °C resulted in an enhanced NO_2 response, with a limit of detection below 50 ppb, and an excellent selectivity against other gaseous like CO, CO_2, C_6H_6 and H_2. Remarkably, the hybrid nanomaterial is characterized by showing significantly faster response and recovery times than those often found in the literature.

1. Introduction

The concentration of hazardous gases shows a constantly rising trend in our environment as a result of the increase in industrial activity [1] and vehicle emissions [2]. The industrialization-related environmental damage is exposing the vast majority of the Earth's population to unhealthy air. One of the most widespread noxious gases is NO_2, which has multiple adverse effects on human health, including the onset of respiratory disorders or skin conditions. The long-term exposure of populations to NO_2 has been related to increased mortality rates [3,4]. The U.S. Environmental Protection Agency (U.S. EPA) has also specified the average exposure limit of NO_2 within one year, which is 53 ppb [5]. Therefore, it is crucial to develop affordable sensors for the widespread detection of NO_2.

Although metal oxide semiconductor (MOS) based sensors, which have been marketed for a long time, show high sensitivity towards NO_2, they suffer from significant disadvantages such as poor selectivity and high working temperatures [6]. In the deployment of an NO_2 monitoring network with high granularity, the access to the power grid is not always easy and this triggers the need of developing battery-operated sensor systems, for which the use of power-hungry sensors is unpractical.

Recently, 2D materials such as transition metal dichalcogenide (TMDs), transition metal monochalcogenides (TMMs), graphene, black phosphorus, and others [7] have emerged as promising candidates in the field of gas sensing. These materials come with some fascinating characteristics, such as enhanced photoelectric properties, thin film dependent physical properties, a high on/off ratio, an abundance of reactive sites or a high surface to volume ratio, only to cite a few [8–10].

Among these materials, InSe stands out as an important III-VI group, layered semiconductor with advanced photoelectric properties. InSe has three polymorphs: ε, which has an indirect bandgap of approximately 1.4 eV; β, which has a direct bandgap of around 1.28 eV in bulk form, and γ, which features a direct bandgap of 1.29 eV. When InSe is in monolayer form, its bandgap for the β polymorph increases significantly from about 1.28 eV to approximately 2.11 eV [11–13]. The bandgap changes from indirect to direct as the thickness of InSe increases to more than six monolayers [14–16]. There literature states different reasons for this behavior: a) The strong quantum confinement in few-layer InSe,

This article is part of a special issue entitled: ICSM2024 published in Materials Today Chemistry.

* Corresponding author. Universitat Rovira i Virgili, MINOS, School of Engineering, Avda. Països Catalans 26, 43007, Tarragona, Spain.
E-mail address: eduard.llobet@urv.cat (E. Llobet).

https://doi.org/10.1016/j.mtchem.2025.103022
Received 25 April 2025; Received in revised form 23 August 2025; Accepted 28 August 2025
Available online 1 September 2025

which causes the valence band maxima to lie away from the Γ point, making the bandgap indirect [17]; b) The occurrence of interlayer coupling in thicker films. As more layers are added (>6), interlayer interactions hybridize electronic states, especially near the Γ point in the Brillouin zone, making the bandgap direct in thicker films [17]; c) DFT and photoluminescence studies also confirm that the PL intensity increases significantly beyond ~6 layers due to direct-gap recombination [18]. Additionally, InSe exhibits high on/off ratios [19] and remarkable carrier mobility, reaching approximately 1000 $cm^2\ V^{-1}s^{-1}$ at room-temperature (RT) [20]. Some other notable electronic properties of InSe are its good stability and excellent photoresponsivity, covering a broad spectral range from the UV to near-infrared [20,21]. It exhibits superior gas sensing and photoelectric performance when stacked randomly instead of in a single crystal orientation [22,23].

Graphene, a 2D carbon material with a honeycomb structure and sp2 hybridization, has been explored extensively in gas sensing applications. It possesses outstanding optical [24,25] and electrical properties [26]. Moreover, graphene exhibits ultrafast optical response time, an ultra-high ballistic transport effect, and thus ultra-high carrier mobility. Due to these characteristics, graphene and InSe are among the promising materials for a new generation of gas sensors. InSe and graphene nanosheets can be produced using various techniques, including liquid phase exfoliation (LPE), chemical vapor deposition (CVD), and mechanical exfoliation (ME). However, techniques like CVD and ME have disadvantages such as high costs and low scalability, respectively. In contrast, LPE [27–31] offers excellent scalability and low cost for producing few-layer 2D materials (i.e., layered nanosheets) when compared to other techniques.

Very few works can be found in the literature demonstrating optoelectronic InSe-based gas sensors for detecting NO_2. Lu Zhang et al. [32] reported a gas sensor based on InSe nanosheets with sensitivity towards NO_2. But the recovery time reported by Lu Zhang and co-workers is rather high (i.e., 1400 s). Qiaoyan Hao et al. [33] reported 1D nano scrolls of InSe activated with visible light that were highly sensitive to NO_2. However, the limit of detection (LoD) for this device lies above 100 ppb, which is a value clearly above the safe exposure limit recommended by the US EPA. Jin-Le-Fan et al. [34] reported a UV-light assisted gas sensor based on the $PdSe_2$/InSe heterojunction with high sensitivity towards NO_2 down to ppb levels. However, its high recovery time (i.e., 1078 s) represents a limitation for the practical use of this sensor. Wei Zheng et al. [35] presented InSe nanosheets for the photoelectrical detection of NO_2 reporting high responses. However, this works reports a response of 2.75 for 10 ppm of NO_2, which is clearly too high a concentration, considering the high toxicity of this gaseous species. Once more, the verified LOD reported for NO_2 is clearly above safe exposure levels.

In this paper, we present a UV light assisted hybrid InSe-graphene gas sensor. We produced InSe and graphene nanosheets using the LPE method and characterized our sensing material using field emission scanning electron microscopy (FESEM), atomic force microscopy (AFM), high resolution transmission electron microscopy (HRTEM), X-ray diffraction (XRD), Raman spectroscopy, energy dispersive X-ray (EDX) and X-ray photoelectron spectroscopy (XPS). Our sensor was tested at RT in the dark and under three different light excitation wavelengths. Additionally, the sensor was tested under mild heating for different NO_2 concentrations at ppb levels. We found that 150 °C is the optimal working temperature under UV light assistance. Under these conditions, our sensor shows unprecedently high response to NO_2 and significantly faster response and recovery times than those reported in the literature.

2. Experimental section

2.1. Materials synthesis and sensor fabrication

InSe powder (99.995 %, CAS#1312-42-1) was purchased from Ossila, Spain and graphene nanopellets (CAS-1034343-98-0) were purchased from STREM Chemicals, USA and were used further for liquid phase exfoliation. A total of 3 ml of 99.5 % 2 propanol from Alfa Aesar and 7 ml of DI water were combined with 5 ml of InSe and 5 ml of graphene. To create a uniform solution at 30 °C, this suspension was sonicated for 8 h. Graphene and InSe nanosheets were exfoliated in this process. Further, the sonicated solution underwent centrifugation to divide the precipitate and the exfoliated nanosheets. After that, the solution was instantly drop casted onto alumina transducers that had a meander heater on the back and interdigitated electrodes on the front (electrode spacing of 300 μm). Alumina transducers were purchased from Ceram Tech GmbH in Plochingen, Germany. Drop casting was used to provide the required baseline resistance and a uniform thin layer on the electrode area. During the process, the transducer alumina substrates were placed on a hotplate set to 80 °C, which enabled the fast evaporation of the solvents, and 110 μl of the solution were drop casted. Supporting Information S1 illustrates the sensor preparation. While InSe films coating the interdigitated electrode area show very high, electrical resistances of typically a few GOhms, the InSe-graphene hybrids show significantly lower resistances (typically of hundreds of Ohms). This characteristic makes the latter suitable for developing chemoresistive devices. A more detailed description of the material preparation and sensor fabrication, can be found in Ref. [36].

2.2. Gas sensing characterization setup

The fabricated sensors were positioned within a 35 ml Teflon chamber able to host up to 4 sensors. The Supporting Information S2 shows a schematic illustration of gas sensing setup. The volume of the test cell is 25 cm^2 (i.e, 25 ml). The cover lid of the chamber was machined to enable connecting ultra-bright LEDs (Thorlabs, model 370E, 375 nm wavelength, 2.5 mW; Thorlabs M470 L5 - 470 nm, 809 mW and Thorlabs M530L4 - 530 nm, 370 mW), in front of the electrode area of every gas sensor device. This Teflon chamber was coupled to a gas mixture and delivery system that provides different concentrations of gases for testing using Bronkhorst mass flow controllers. Calibrated gas bottles with gases balanced in dry air were employed (i.e., NO_2, CO_2, CO, H_2, and C_6H_6). Dry air was used as the carrier gas and a constant flow of 100 ml/min was kept throughout the measurements. Such a flow rate means that the entire volume of gas in the test chamber was replaced every 15 s (i.e., 25 ml ÷ 100 ml × min^{-1} = 0.25 min = 15 s). Before starting the measurements, sensors were kept in the chamber for 5 h under a flow of dry air in order to stabilize their baseline resistance. A typical measurement consisted of exposing the sensors to 10 min of the desired gas concentration followed by 30 min recovery in dry air. The sensor responses were measured when sensors were operated either at room temperature or at 150 °C, under dark or under light excitation (at three different wavelengths). Sensor responses were calculated using equation (1) for oxidizing gases and equation (2) for reducing gases:

$$R\% = \left(R_{air} - R_{gas}\right) / R_{air} \times 100 \quad (1)$$

$$R\% = \left(R_{gas} - R_{air}\right) / R_{air} \times 100 \quad (2)$$

where R_{air} and R_{gas} are the sensor resistances in dry air (i.e., baseline resistance) and in the presence of a gas, respectively.

2.3. Physicochemical characterizations

FESEM, AFM, HRTEM, XRD, Raman, XPS and EDX were utilized to investigate the morphological and structural properties and the chemical composition of bulk InSe and the sensing film. Thermo Scientific Scios 2 field emission scanning electron microscope with focused ion beam was utilized to examine how the bulk InSe orientation changed before and after exfoliation. The atomic force microscope Agilent 5500 was used with intermittent contact (Tapping mode) to analyze the thickness of the sensing layer. High resolution transmission electron

microscope from JOEL, with F200 TEM ColdFEG was operated at 200 kV for studying the morphological structures of nanosheets and Fourier transform SAED was performed to study the crystallographic structure of the sensing films. The crystal structure was analyzed using X-ray diffraction equipped with a vertical θ-θ goniometer, XYZ motorized stage, parallel incident beam (Globel mirror) and a general area diffraction system (GADDS) from the Bruker AXS D8 ADVANCE diffractometer. The Raman spectra were recorded using a Renishaw in Via, equipped with a 633 nm argon laser -Novatech 25 mW. Energy Dispersive X-ray elemental mapping was performed from Quanta 600 ESEM microscope from FEI Company. The ESEM microscope uses electron beam to form the image. It features high resolution (3 nm) and a deep depth of field, allowing it to focus on different heights of the sample simultaneously. This ESEM can perform various functions such as - topographic imaging, atomic number contrast imaging and energy-dispersive X-ray spectrometry. The X-ray photoelectron spectroscopy analysis was carried out to confirm the presence of elements and to investigate their oxidation states on the surface of the synthesized hybrid material. XPS analysis was performed using an **ProvenX-NAP** (Specs Surface Nano Analysis GmbH, Berlin, Germany) spectrometer with a dual (AlKα = 1487 eV/AgLα = 2984 eV) monochromatic X-ray source (μFocus450).

3. Results and discussion

3.1. Materials characterization results

The hybrid InSe-graphene hybrid was obtained using the LPE approach, as described in the preparation process. FESEM analysis was performed to investigate the morphology of the bulk InSe and the hybrid InSe-graphene film coating the electrode area of an alumina substrate, as shown in Fig. 1(a). The FESEM images revealed that the bulk InSe is properly stacked in multilayers, whereas the exfoliated hybrid InSe-graphene nanosheets are randomly dispersed on the electrode surface. After the LPE process, the bulk material, with large sheets, the length of which lies approximately in the micrometer range, has been transformed into nanometer-sized flakes, shown in Fig. 1(b). It is well known that exfoliated monolayers perform exceptionally well photoelectrically when layered randomly [37].

Fig. 1(c and d) displays an AFM image of hybrid InSe-graphene nanosheets on a silicon wafer, showing an average thickness of 1.79 μm. The image indicates the presence of multilayered stacks of exfoliated nanosheets. According to previous reports, InSe exhibits a direct bandgap structure when endowed with more than ~6–7 monolayers, which enhances light absorption and in turn increases the photoelectric response [17].

A solution of the exfoliated hybrid was drop casted onto a TEM copper grid to obtain transmission electron micrographs. Fig. 1(f) displays the array pattern of the exfoliated sheets. Fig. 1(e) shows the exfoliated nanosheets with distinct edges arranged one on top of the other. The inset in Fig. 1(e) shows the SAED having a distinct hexagonal atomic pattern of graphene with scattered spots, which can be attributed to the structural deformation of InSe in graphene.

Fig. 1(g), depicts the XRD data recorded to study the crystallographic structure of the hybrid. Samples were placed directly on the sample holder and the area of interest was selected with the aid of a video-laser focusing system. An X-ray collimator system allows to analyze areas of 500 μm. The X-ray diffractometer was operated at 40 kV and 40 mA to generate $Cu_k\alpha$ radiation. The GADDS detector was a VÅNTEC-500 (silicon strip technology of 30 × 30 cm with 2048 × 2048 pixels) placed at 15 cm from the sample. We collected three frames in omega-scan mode (2D XRD patterns) covering 8–92° 2θ. The exposure time was 600 s per frame and it was chi-integrated to generate the conventional 2θ vs. intensity diffractogram. The XRD diffractogram for the hybrid nanomaterial was analyzed using ICDD card number- 34–1434 for InSe, ICDD card number- 75–2078 for graphene and ICDD card number- 034–1431 for Al_2O_3 corundum. InSe was found to be in the hexagonal phase in $P6_3/mmc$ space group and graphene was found to be in rhombohedral phase in R-3m space group. Peaks found for InSe, graphene and alumina corundum are [(006), (105), (110), (114), (0012)], [(101), (110), (107)] and [(104), (006), (024), (116), (018), (214), (300)] respectively. which correspond to 2θ = [21.29°, 25.68°, 32.25°, 37.44°, 45.30°, 50.52°,67.52°], [43.45°, 77.69°and 80.73°] and [35.15°,41.6°, 52.55°, 57.50°, 61.22°, 66.4°,68.20°] respectively. The Al_2O_3 corundum exists in the rhombohedral lattice of R-3c (167) space group with lattice parameters a = b = 4.75 and c = 12.99. Fig. 1(h) depicts the Raman spectrum of the hybrid InSe-graphene. Raman scan was performed in the range of 15 cm^{-1} to 300 cm^{-1}. Laser exposure power and accumulation time were set to 10 % and 100 s, respectively.

The Raman results for InSe and graphene are displayed in the separate insets within panel *h* of Fig. 1 due to the differences in intensity and for clear understanding. In InSe a total of 7 vibrational modes are present, out of which five are active in this hybrid which are - E′, E″, $A_1^{'}$, E" and $A_1^{'}$. These modes correspond to the 17 cm^{-1}, 41 cm^{-1}, 114 cm^{-1}, 175 cm^{-1} and 221 cm^{-1} Raman shifts. These active modes confirm that InSe exists in β polytype [38,39]. For graphene, Raman peaks D, G, 2D, D + G and 2G bands are active. Band D at 1370 cm^{-1} indicates the strength of graphene damage, band G at 1399 cm^{-1} depicts the amount of graphitic content in solution, and bands 2D at 1568 cm^{-1} and 2G at 1565 cm^{-1} represent the secondary peaks of graphene disruption and graphitic content, respectively [40]. The intensities of the graphene disruption peaks indicate that the sample is not heavily impacted due to the exfoliation process and that the graphitic structure remains intact. Raman results confirm the presence of both elements (i.e., InSe and graphene) in the sample. EDX data was acquired from multiple spots on the sample, and the aggregate of all locations was used to calculate the exact average weight% and atomic% for each element. Please refer to Supporting Information S3 for the average weight % and atomic% percentage for each element and the EDX spectrum of the InSe and graphene sample. EDX elemental mapping validates the existence of all elements and justifies the quantities utilized to synthesize the sensing layer, which were 5 mg for InSe and graphene, respectively.

An XPS analysis of the sensing material was performed to study the surface elemental composition present. The measurements were collected under the following conditions: 100 W power (AlKα anode), the hemispherical analyzer operating in the main fixed analyzer transmission mode, entrance slit of 7 × 20 mm and exit slit open with mesh. The data were recorded with a PHOIBOS 150 NAP 1D-DLD and the total pressure in the main vacuum chamber during analysis was better than $2{\cdot}10^{-9}$ mbar. Survey spectrum was collected at 80 eV of pass energy and 0.7 eV of step size. The InSe-graphene hybrid constitutes of In 3.00 %, Se 2 %, O 15.11 %, C 73.82 % and Si from substrate 6.82 % according to atomic weight percentage of the sample. Fig. 2 (a) shows the recorded survey spectrum. Fig. 2 (b) shows the high resolution spectrum for the In3d region in which two main peaks have been observed at 445.4 eV (In3d5/2) and 452.9 eV (In3d3/2). This value of BE (445.3eV) has been reported in the literature for adsorbed oxygen on the In surface [41]. This adsorption of oxygen is due to prolonged sonication process the material underwent during the exfoliation step, as already reported [42,43]. Fig. 2 (c) shows the high-resolution spectrum in the Se3 region. Four peaks can be observed at 54.5 eV (Se3d5/2) and 55.4 eV (Se3d3/2), and 55.5 eV (Se3d5/2) and 56.3 eV (Se3d3/2). The binding energy at 54.5 eV confirms that selenium is in the Se^{2-} oxidation state (InSe). The other value at 55.5 eV could correspond to partially oxidized Se, considering the adsorbed water on the surface and the presence of –OH species found in the O1s region. This value has been reported in the literature to belong to metallic Se. When a slight superficial degradation of InSe happens, elemental Se (Se0) can be formed, which is in agreement with what has been observed. This spectrum also confirms that there are no SeO_2 species, as its corresponding feature around 59 eV does not appear in the high resolution spectrum [44]. Fig. 2 (d) shows the auger Se + C region peaks. In this region, 5 different components

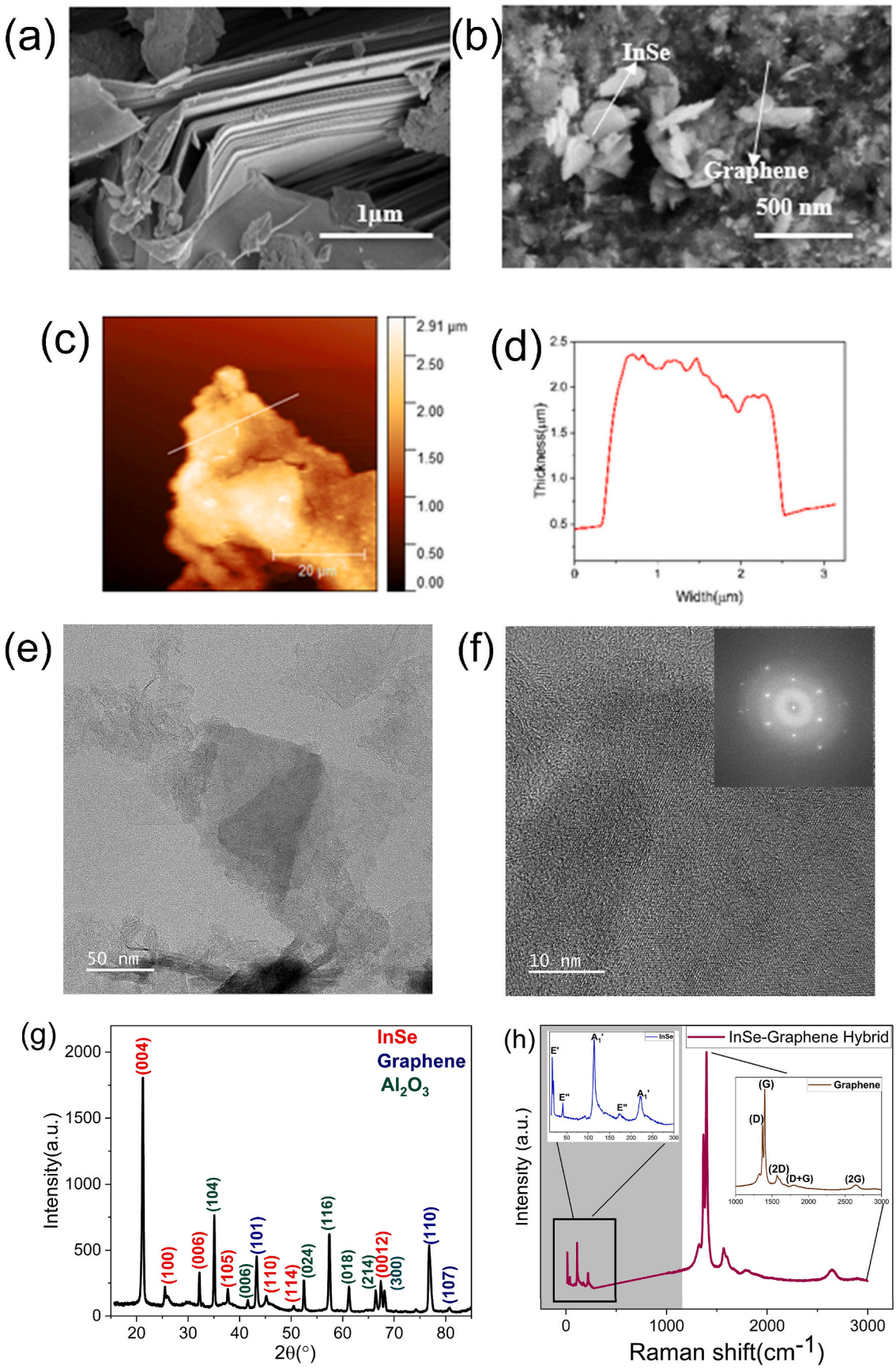

Fig. 1. (a) FESEM image for bulk InSe. (b) FESEM image for exfoliated flakes of hybrid InSe-graphene. (c–d) AFM images of exfoliated flakes of hybrid InSe-graphene with measured thickness. (e–f) HRTEM images of hybrid InSe-graphene. (g). XRD diffractogram for the hybrid InSe-graphene sample. (h). Raman spectrum for the hybrid InSe-graphene sample.

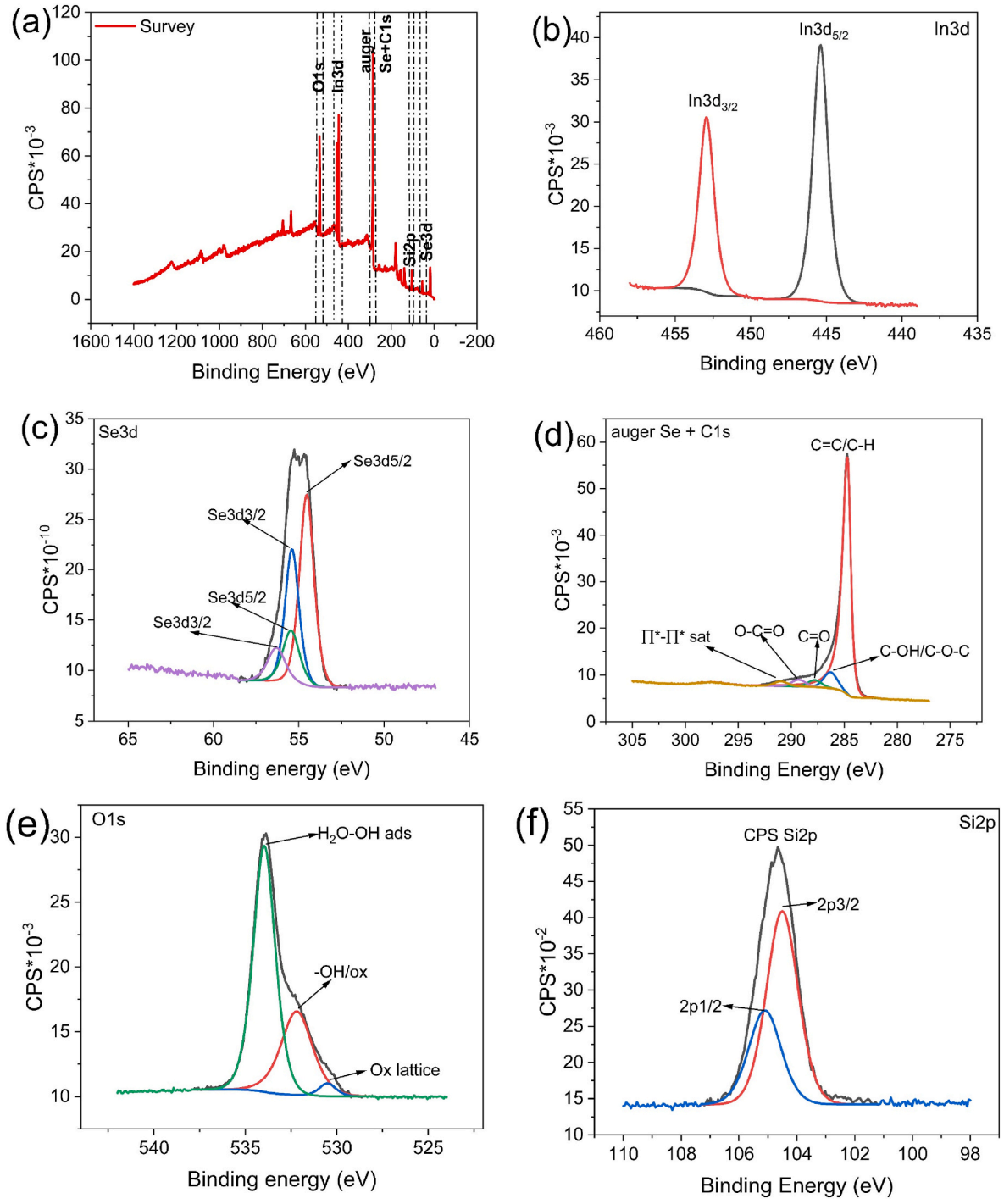

Fig. 2. XPS analysis for InSe-graphene hybrid showing (a). Complete Survey of the sample (b). In3d region peaks (c). Se3d region peaks (d). auger Se + C1s region peaks (e). O1s region peaks (f). Si2p region peaks.

have been observed at 284.8 eV, 286.3 eV, 287.8 eV, 289.3 eV and 291.0 eV. These values can be associated with C═C/C–H/C–C, C–OH/C–*O*–C, C═O, O–C═O and Π* - Π* satellite [45]. Fig. 2 (e) shows the In O1s region, three components have been observed at 530.5, 532.2 and 534.0 eV. These values could be associated with oxygen lattice (In_2O_3), –OH/ox. defects and H_2O -OH adsorbates, respectively [46]. Fig. 2 (f) shows the high resolution spectrum for the Si2p region. In this region two main peaks have been observed at 104.5 eV (Si2p3/2) and 105.1 eV (2p1/2). This value has been reported in literature to be associated with Si–O bonds (Si4+) [47].

3.2. Gas sensing results

The hybrid InSe-graphene sensor was tested toward 1 ppm NO_2 gas at RT (25 °C) in the dark and under three different light excitation wavelengths (365 nm for UV excitation, 470 nm for blue excitation, and 530 nm for green excitation), as shown in Fig. 4(a) and also at the Supporting Information S5. On exposure to different light sources, in contrast to the dark operation, a significant improvement in responsiveness is observed. Particularly, in the presence of UV light, response increases from 1.74 % to 2.75 %. This enhancement can be attributed to UV radiation generating numerous electron-hole pairs showing the

greatest resistance drop in the sensing device. The photoexcited electrons may increase NO_2 adsorption, while the interaction of photoexcited holes with negatively charged NO_2 could facilitate desorption. This interaction may alter the material's electrical properties, rendering it more receptive to gas molecules [32,34,48]. Additionally, we assessed the behavior of our sensor in the dark and during UV exposure while being heated at moderate temperatures of 50, 100 and 150 °C. These results are shown in Fig. 3 and indicate that 150 °C is the operating temperature in which a higher response is achieved. The sensor was not tested at operating temperatures above 150 °C as this would have increased the risk of degrading the sensor surface via promoting oxidation processes. Fig. 4(b) shows the response dynamics curves for the sensor operated at 150 °C under either dark or UV excitation conditions. In addition to improving the sensor's response, especially when combined with UV exposure, heating also ameliorated substantially the problem of mild linear baseline drift that was experienced during room temperature operation. The baseline drift can be attributed to the fact that, under continuous UV exposure, adsorbed NO_2 or other ambient species (like O_2 or H_2O) can desorb from the surface of InSe and graphene. This cleaning effect leads to a lower density of surface charges, reducing the baseline conductivity as reported in Refs. [49,50]. Additionally, a slight drift remains visible under UV light, this can be attributed to the fact that a continuous exposure to UV light can lead to intrinsic photo-doping of the graphene or InSe layer [51]. This strategy of raising the operating temperature to the sensor is conventional in metal oxide-based NO_2 gas sensors [52,53]. In essence, a sensor operating at ambient temperature may have a low response because NO_2 adsorption is a thermally activated process. As the temperature rises from RT to 150 °C, the thermal energy increases, resulting in more thermally excited electrons and more sensitivity than at room temperature (as nitrogen dioxide is an electron acceptor). The sensor response increased from 1.74 % under dark, RT conditions to 7.12 % with the combined effect of UV and temperature.

The exfoliated pristine InSe films show an extremely high resistance (usually in giga Ohms), making the use of pristine InSe nanomaterial films in chemoresistive devices impractical. A sensor employing exfoliated InSe only was prepared as well. Its electrical resistance in clean air was too high to be measured properly with a standard multimeter. This InSe sensor was exposed to NO_2, but the response was sluggish with an extremely low signal to noise ratio. These results can be found in the Supporting Information, S4. It was to solve the issue of having too high a resistance, that employing an InSe/graphene hybrid material was envisaged. However, this strategy not only enhances clearly the conductivity of the resulting hybrid material, but also enables improving the sensing performance of pure InSe or the one of pristine graphene sensors. For instance, F. Yavari reported a pristine graphene sensor detecting NO_2 and NH_3, which showed a response of 4 % to 0.1 ppm of NO_2 at 200 °C with 3000 s response and recovery times [54]. X. Yan reported a pristine graphene, UV-assisted sensor detecting 100 ppm of NO_2 at RT under a 265 nm UV light excitation. The response intensity was 26 % and the response and recovery times were 200 s and 1000 s, respectively [55]. The hybrid InSe-graphene sensor outperforms pristine graphene sensors in terms of sensitivity, selectivity, response/recovery time, and limit of detection (LoD).

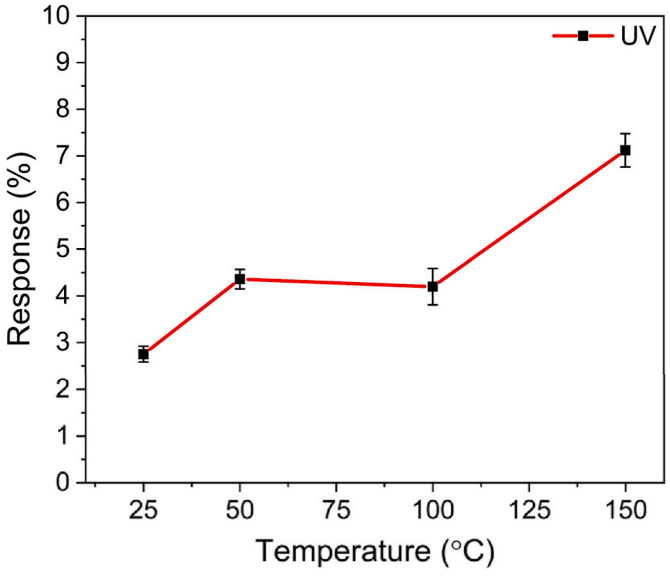

Fig. 3. Effect of the sensor operating temperature in its response towards 1 ppm of NO_2 under UV light excitation.

Thus, the hybrid sensor was investigated further for detecting lower concentrations of NO_2, which ranged from 50 ppb to 1 ppm. Again, the sensor was operated either at RT or at 150 °C, in the dark or under UV excitation. These results are summarized in Fig. 4(c). A drastic improvement in response was observed when the sensor was operated under continuous UV excitation and mild heating to 150 °C. The limit of detection for the sensor is also experimentally confirmed to be below 50 ppb of NO_2. Additionally, Fig. 5(a) clearly compares the responses with varying NO_2 concentrations under these two operating conditions, elucidating the combined effect of temperature and UV excitation.

In addition to NO_2, the cross sensitivity of the sensor was investigated to reducing gases, such as CO, H_2, C_6H_6 and CO_2. The responses for CO (50 ppm), H_2 (1000 ppm), C_6H_6 (1 ppm) and CO_2 (1000 ppm) are shown in Fig. 5(b). All these gases were tested under the same conditions of our best response to NO_2, i.e., under UV excitation and at an operating temperature of 150 °C. The sensor response was found to be much higher for NO_2 compared to any other gas tested. While for all the gases but not NO_2, sensor response remains below 1 %, for 1 ppm of NO_2 the response is 7.12 %. This can be attributed to the fact that, in comparison to other gas molecules, NO_2 has a higher adsorption energy (−0.24 eV) and a charge transfer (−0.039 e) in InSe This explains the selectivity of the sensor towards NO_2 [56,57]. The dynamic sensor responses upon the exposure to these potentially interfering species can be found in the Supporting Information S6.

Furthermore, as shown in Fig. 5(c and d), the response and recovery times under dark conditions at 150 °C and under UV light at 150 °C were calculated. Under dark, the response and recovery times were 108 and 325 s, respectively. Under UV light excitation, response and recovery remained virtually unchanged. The sensor responses under UV light combined with heating increased, but response and recovery times remained unchanged. For sensor response and recovery time curves under UV light and RT operation, please see the Supporting Information S7. Even though the cross-sensitivity towards humidity of InSe/graphene operated at 150 °C and under UV excitation has not been tested, previous results reported for InSe/graphene at 150 °C and under dark conditions let us anticipate that the sensitivity towards NO_2 would increase if background humidity levels were increased [36]. The sensor long-term stability has also been tested for the period of over 4 weeks, and the responses are presented in Fig. 6. Initial long-term stability results show that a decrease in sensor response appears in the early stages and then a tendency to achieve stability over time is observed. This could be due to certain factors like degradation of sensor surface with ambient environment and impurities adsorbed on the surface over time. Additionally, the response intensity towards NO_2, response and recovery times, and limit of detection (LOD) of the InSe-graphene hybrid sensor presented here have been compared to those of other hybrid sensing materials and pure graphene from the literature. These results are summarized in Table 1. The response intensity reported in the literature is for NO_2 concentrations ranging from 5 to 100 ppm, and the reported LOD are higher than 50 ppb. In contrast, our InSe-graphene sensor has demonstrated a higher response, even for NO_2 concentrations lower than 1 ppm, and the LOD is clearly below 50 ppb. Furthermore, the response and recovery times for the InSe-graphene sensor compare

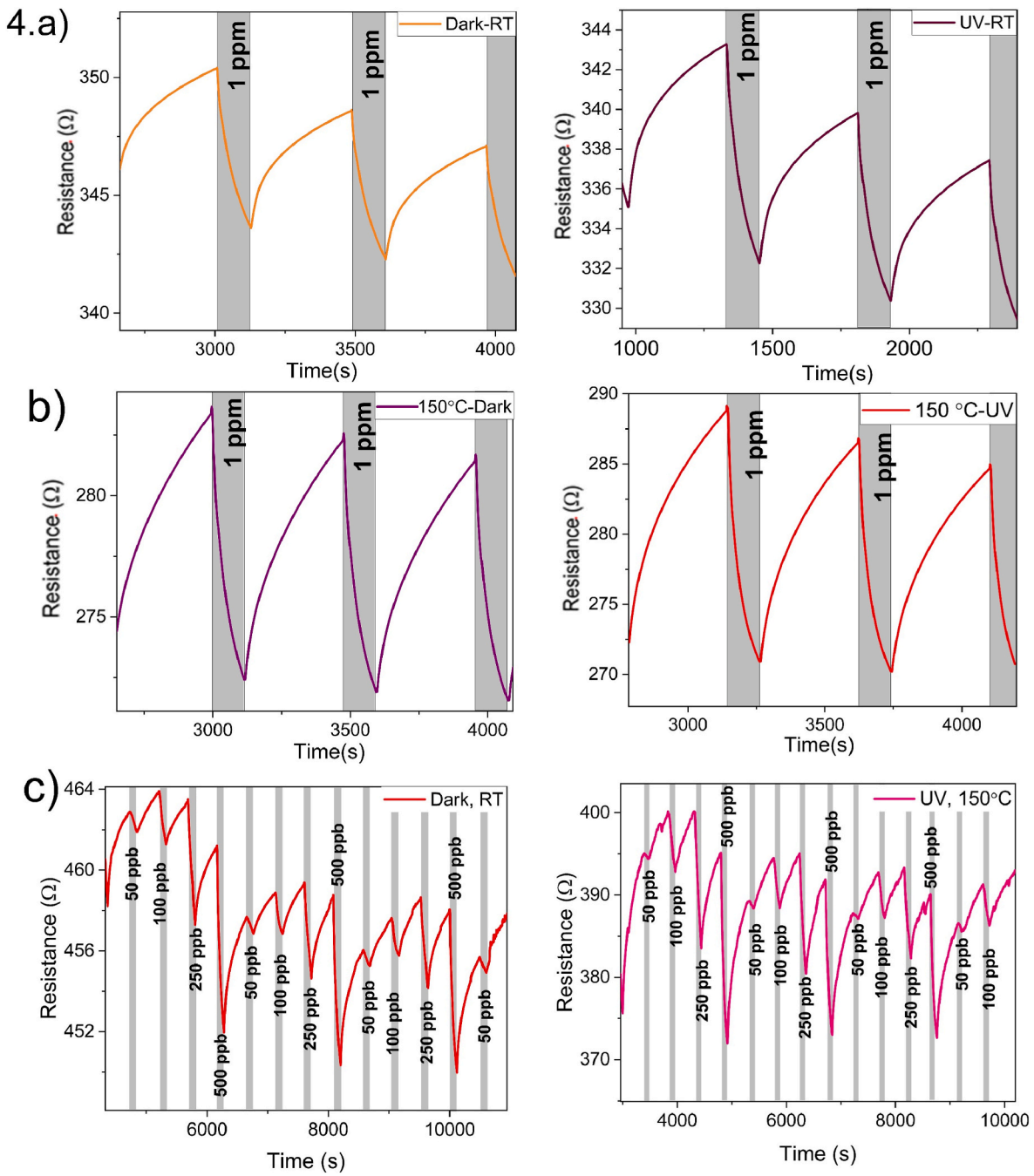

Fig. 4. (a) Hybrid InSe-graphene sensor response towards 1 ppm NO2 in presence and absence of UV light at RT. (b). Sensor response in dark and in UV light at optimum temperature towards 1 ppm NO2. (c). Sensor response towards lower concentrations of NO2 in the dark at RT and in presence of UV light at an operating temperature of 150 °C.

favorably to most of those reported in the literature.

3.3. Sensing mechanism

Theoretical studies conducted on InSe indicate that the adsorption energy of NO_2 is −0.24 eV and that there is a fraction of electronic charge (0.039 e) transferred from the InSe to the NO_2 molecule upon adsorption. Such adsorption energy and associated electronic charge are higher than those estimated for other gas molecules (e.g., CO, NH_3, H_2O, NO) [56,57]. These characteristics suggest that InSe physisorbs NO_2 molecules, and this significantly alters the number of charge carriers, thus, device resistance. InSe behaves as a p-type semiconductor and electron injection towards the NO_2 molecule results in an increased number of holes (i.e., the majority charge carriers), which translates in a resistance drop, when the device is exposed to nitrogen dioxide[64–66]. The material reported here is an InSe/graphene hybrid. Graphene has undergone an exfoliation process implying a long sonication, which is known to inflict some degradation to its structure (i.e, generation of defects) and to promote oxidation [67,68]. Sonicated graphene shows a p-type semiconductor behaviour [36,69–71]. It is known to physisorb NO_2 and, similarly to the InSe case, electronic charge transfer from the graphene towards the adsorbed NO_2 molecule is derived [69,72]. The response towards nitrogen dioxide of pure graphene that had undergone the same exfoliation procedure was reported in Ref. [36], and found to be two times lower than that of InSe/graphene hybrids. This is indicative that the interaction of InSe with NO_2 and the resulting modulation of the

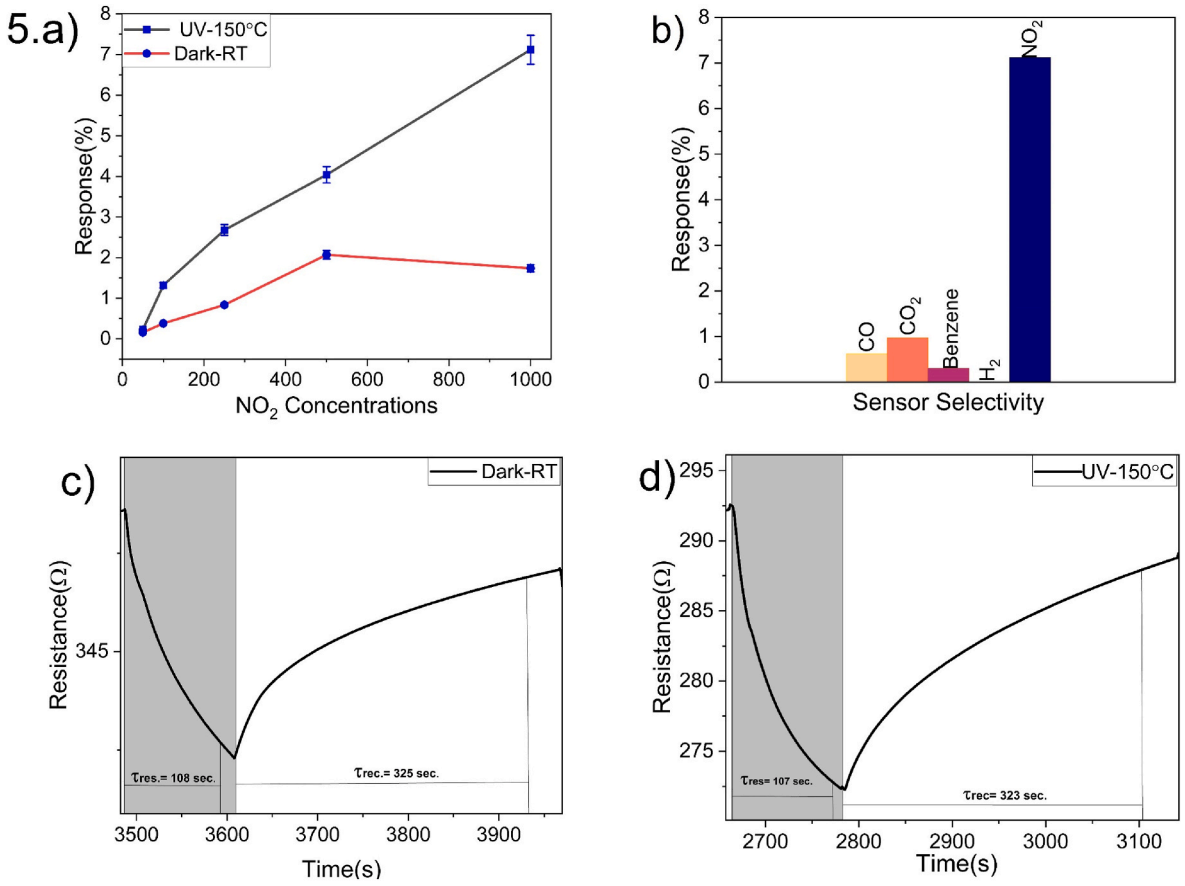

Fig. 5. (a) Hybrid InSe-graphene sensor response comparison towards lower concentrations of NO_2 in presence and absence of UV light at RT and at optimum temperature. (b). Sensor response towards different gases in UV light at optimum temperature. (c). Response and Recovery time in Dark at RT. (d). Response and Recovery time in presence of UV light at optimum temperature.

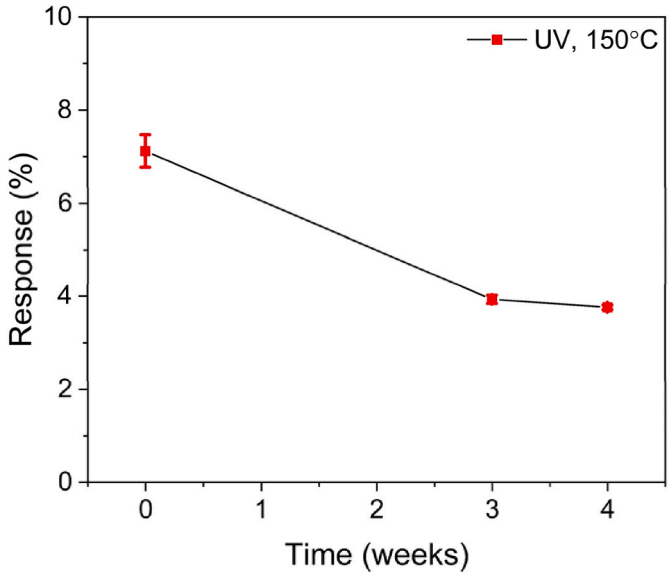

Fig. 6. Long term stability results for InSe-graphene hybrids under optimum measurement conditions.

Schottky barrier height of the *p*-InSe/p-sonicated graphene heterojunctions is essential for achieving this increase in response. When UV irradiation is applied, electron-hole pairs are photogenerated [73]. These charge carriers are separated by the electric field existing between the interdigitated electrodes, since a small DC voltage is applied to measure the device resistance. Photogenerated electrons can then participate in the adsorption of further NO_2 molecules, which results in a significantly increased response in comparison to that of devices operated under dark conditions.

4. Conclusions

A hybrid sensor based on InSe-graphene has been developed. After testing the sensor at three different light excitation wavelengths, we found that the best response was obtained under UV excitation (365 nm), greater than when operated in the dark. We also investigated the 1 ppm NO_2 response at a moderate temperature of 150 °C with and without UV excitation. The responses towards 1 ppm of NO_2 increased from 1.74 % under dark conditions to 7.12 % under UV light and temperature excitation. Results show a limit of detection below 50 ppb, and excellent selectivity. Remarkably, the hybrid nanomaterial is characterized by showing significantly faster response and recovery times than those found in the literature. Therefore, it could be concluded that UV exposure enhances sensor responses and that the best responses occur when mild heating is combined with UV excitation, thus enhancing the overall sensing performance. This enhancement is attributed to UV light generating extra electronic charge carriers that become available for adsorbing further NO_2 molecules.

CRediT authorship contribution statement

Jyayasi Sharma: Writing – original draft, Methodology, Investigation, Formal analysis, Data curation. **Frank Güell:** Writing – review &

Table 1
Comparison of NO_2 sensors based on TMD materials heterostructure.

Sensing Material	Operating Conditions	NO_2Conc. (ppm)	Response	LOD (ppb)	Res/Rec. Time(s)	Gas flow rate/expo–sure time	Ref.
TiO_2/PrGO	RT (365 nm, UV)	100	35.6 %[a]	114[c]	59/33	300 sccm/-	[58]
ZnO/graphene	RT	5	6.78 %[a]	3000[d]	1400/1600	–/–	[59]
SnS_2/Pt_3Sn	RT	50	17.63 %[a]	200[d]	120/1000	-/2 min	[60]
WS_2/PbS	RT (365 nm, UV)	5	9[b]	200[d]	–		[48]
Graphene	200 °C	0.1	4 %[a]	–	3000/3000	-/50 min	[54]
Graphene	RT (265 nm, UV)	100	26 %[a]	42.18[d]	200/1000	1000 sccm/10 min	[55]
InSe nanosheets	RT/UV	10	2.75[b]	100[d]	6/169	–/–	[35]
InSe nanosheets	RT (365 nm, UV)	5	3[b]	50[d]	470/1400	1000 sccm/10 min	[32]
n-MoS2/GaN	RT	50	48.42 %[a]	5000[d]	298/1395	-/10 min	[61]
Ag/p-SnS	RT	20	30 %	500[d]	40/1320	–/–	[62]
PdSe2/InSe	RT (365 nm, UV)	5	2.1[b]	100[d]	275/1078	300 ml^{-1}/-	[34]
In_2S_3	RT	10	21.5	50[d]	200/1480	–/–	[63]
InSe/graphene	Dark, RT	1	1.74 %[a]	<50[d]	108/325	100 sccm/10 min.	This work
	RT (365 nm UV)	1	2.75 %[a]	–	107.1/324		
	150 °C (365 nm, UV)	1	7.12 %[a]	<50[d]	107/323		

[a] $R\% = (R\ air - R\_gas)/R\_air$ *100.
[b] Ra/Rg or Rg/Ra.
[c] Theoretical Calculations.
[d] Experimentally verified.

editing, Supervision. **Mubdiul Islam Rizu:** Investigation. **Dalal Fadil:** Supervision. **Eduard Llobet:** Writing – review & editing, Supervision, Funding acquisition.

Declaration of competing interest

The authors declare that they have no known competing financial interests or personal relationships that could have appeared to influence the work reported in this paper.

Acknowledgements

J.S. is supported by the predoctoral program AGAUR-FI SDUR under grant no. 2022 FI SDUR 00307 of the Department of Research and Universities of the Government of Catalonia and the European Social Plus Fund. This project has received funding from the European Union's Horizon 2020 research and innovation programme under the Marie Sokolowska-Curie grant agreement No 101025770 and by the Spanish Agencia Estatal de Investigación (AEI) and FEDER under grant no. PID2022-142451OB-C21. E.L. is supported by the Catalan Institution for Research and Advanced Studies (ICREA) via the 2023 Edition of the ICREA Academia Award. The authors and the URV would like to thank project EQC2021-007785-P, awarded by the Ministry of Science and Innovation and funded by the European Union (NextGeneration), for the total funding for the acquisition of the XPS system (ProvenX-NAP from SPECS) at the SRCiT of the URV.

Appendix A. Supplementary data

Supplementary data to this article can be found online at https://doi.org/10.1016/j.mtchem.2025.103022.

Data availability

Data will be made available on request.

References

[1] R.M. Agus, A. Mallongi, M. Hatta, A. Syac, A. Muhith, S. Siyoto, M. Saleh, Ambient air quality of SO2 and NO2 in settlements around industrial area of makassar 2019, Enferm. Clin. 30 (2020) 328–332, https://doi.org/10.1016/j.enfcli.2019.10.093.
[2] D.C. Carslaw, N.J. Farren, A.R. Vaughan, W.S. Drysdale, S. Young, J.D. Lee, The diminishing importance of nitrogen dioxide emissions from road vehicle exhaust, Atmos. Environ. X 1 (2019) 100002, https://doi.org/10.1016/j.aeaoa.2018.100002.
[3] H. Kasuga, Health effects of air pollution, how to Conquer air Pollut, a Japanese Exp (1989) 95–113, https://doi.org/10.1016/s0272-5231(21)00851-0.
[4] U. Latza, S. Gerdes, X. Baur, Effects of nitrogen dioxide on human health: systematic review of experimental and epidemiological studies conducted between 2002 and 2006, Int. J. Hyg Environ. Health 212 (2009) 271–287, https://doi.org/10.1016/j.ijheh.2008.06.003.
[5] T. Pham, G. Li, E. Bekyarova, M.E. Itkis, A. Mulchandani, MoS 2 -Based optoelectronic gas sensor with sub-parts-per-billion limit of NO 2 gas detection, ACS Nano 13 (2019) 3196–3205, https://doi.org/10.1021/acsnano.8b08778.
[6] R. Kumar, X. Liu, J. Zhang, M. Kumar, Room-Temperature Gas Sensors Under Photoactivation: from Metal Oxides to 2D Materials, Springer Singapore, 2020, https://doi.org/10.1007/s40820-020-00503-4.
[7] V. Shanmugam, R.A. Mensah, K. Babu, S. Gawusu, A. Chanda, Y. Tu, R.E. Neisiany, M. Försth, G. Sas, O. Das, A review of the synthesis, properties, and applications of 2D materials, Part. Part. Syst. Charact. 39 (2022), https://doi.org/10.1002/ppsc.202200031.
[8] E. Lee, Y.S. Yoon, D.J. Kim, Two-dimensional transition metal dichalcogenides and metal oxide hybrids for gas sensing, ACS Sens. 3 (2018) 2045–2060, https://doi.org/10.1021/acssensors.8b01077.
[9] G.R. Bhimanapati, Z. Lin, V. Meunier, Y. Jung, J. Cha, S. Das, D. Xiao, Y. Son, M. S. Strano, V.R. Cooper, L. Liang, S.G. Louie, E. Ringe, W. Zhou, S.S. Kim, R.R. Naik, B.G. Sumpter, H. Terrones, F. Xia, Y. Wang, J. Zhu, D. Akinwande, N. Alem, J. A. Schuller, R.E. Schaak, M. Terrones, J.A. Robinson, Recent advances in two-dimensional materials beyond graphene, ACS Nano 9 (2015) 11509–11539, https://doi.org/10.1021/acsnano.5b05556.
[10] R. Vargas-Bernal, Electrical properties of two-dimensional materials used in gas sensors, Sensors (Switzerland) 19 (2019) 100–107, https://doi.org/10.3390/s19061295.
[11] N. Curreli, M. Serri, D. Spirito, E. Lago, E. Petroni, B. Martín-García, A. Politano, B. Gürbulak, S. Duman, R. Krahne, V. Pellegrini, F. Bonaccorso, Liquid phase exfoliated indium selenide based highly sensitive photodetectors, Adv. Funct. Mater. 30 (2020), https://doi.org/10.1002/adfm.201908427.
[12] M. Brotons-Gisbert, D. Andres-Penares, J. Suh, F. Hidalgo, R. Abargues, P. J. Rodríguez-Cantó, A. Segura, A. Cros, G. Tobias, E. Canadell, P. Ordejón, J. Wu, J. P. Martínez-Pastor, J.F. Sánchez-Royo, Nanotexturing to enhance photoluminescent response of atomically thin indium selenide with highly tunable band gap, Nano Lett. 16 (2016) 3221–3229, https://doi.org/10.1021/acs.nanolett.6b00689.
[13] J. Camassel, P. Merle, H. Mathieu, A. Chevy, Excitonic absorption edge of indium selenide, Phys. Rev. B 17 (1978), https://doi.org/10.1103/PhysRevB.17.4718.
[14] G.W. Mudd, M.R. Molas, X. Chen, V. Zólyomi, K. Nogajewski, Z.R. Kudrynskyi, Z. D. Kovalyuk, G. Yusa, O. Makarovsky, L. Eaves, M. Potemski, V.I. Fal'Ko, A. Patanè, The direct-to-indirect band gap crossover in two-dimensional van der Waals Indium Selenide crystals, Sci. Rep. 6 (2016) 1–10, https://doi.org/10.1038/srep39619.
[15] S. Lei, L. Ge, S. Najmaei, A. George, R. Kappera, J. Lou, M. Chhowalla, H. Yamaguchi, G. Gupta, R. Vajtai, A.D. Mohite, P.M. Ajayan, Evolution of the electronic band structure and efficient photo-detection in atomic layers of InSe, ACS Nano 8 (2014) 1263–1272, https://doi.org/10.1021/nn405036u.
[16] G.W. Mudd, S.A. Svatek, T. Ren, A. Patanè, O. Makarovsky, L. Eaves, P.H. Beton, Z. D. Kovalyuk, G.V. Lashkarev, Z.R. Kudrynskyi, A.I. Dmitriev, Tuning the bandgap of exfoliated InSe nanosheets by quantum confinement, Adv. Mater. 25 (2013) 5714–5718, https://doi.org/10.1002/adma.201302616.
[17] M.J. Hamer, J. Zultak, A.V. Tyurnina, V. Zólyomi, D. Terry, A. Barinov, A. Garner, J. Donoghue, A.P. Rooney, V. Kandyba, A. Giampietri, A. Graham, N. Teutsch, X. Xia, M. Koperski, S.J. Haigh, V.I. Fal'Ko, R.V. Gorbachev, N.R. Wilson, Indirect to direct gap crossover in two-dimensional InSe revealed by angle-resolved

photoemission spectroscopy, ACS Nano 13 (2019) 2136–2142, https://doi.org/10.1021/acsnano.8b08726.
[18] N.A. Pike, R. Pachter, M.A. Altvater, C.E. Stevens, M. Klein, J.R. Hendrickson, H. Zhang, S. Krylyuk, A.V. Davydov, N.R. Glavin, Understanding the origin and implication of the indirect-to-direct bandgap transition in multilayer InSe, J. Phys. Chem. C 128 (2024) 7957–7967, https://doi.org/10.1021/acs.jpcc.4c01104.
[19] W. Feng, W. Zheng, W. Cao, P. Hu, Back gated multilayer InSe transistors with enhanced carrier mobilities via the suppression of carrier scattering from a dielectric interface, Adv. Mater. 26 (2014), https://doi.org/10.1002/adma.201402427.
[20] D.A. Bandurin, A. V Tyurnina, G.L. Yu, A. Mishchenko, V. Zólyomi, S. V Morozov, R.K. Kumar, R. V Gorbachev, Z.R. Kudrynskyi, S. Pezzini, Z.D. Kovalyuk, U. Zeitler, K.S. Novoselov, A. Patanè, L. Eaves, I. V Grigorieva, V.I. Fal'Ko, A.K. Geim, Y. Cao, High electron mobility, quantum hall effect and anomalous optical response in atomically thin InSe, Nat. Nanotechnol. 12 (2017), https://doi.org/10.1038/nnano.2016.242.
[21] W. Feng, J. Bin Wu, X. Li, W. Zheng, X. Zhou, K. Xiao, W. Cao, B. Yang, J.C. Idrobo, L. Basile, W. Tian, P.H. Tan, P.A. Hu, Ultrahigh photo-responsivity and detectivity in multilayer InSe nanosheets phototransistors with broadband response, J. Mater. Chem. C 3 (2015) 7022–7028, https://doi.org/10.1039/c5tc01208b.
[22] Y. Yu, S. Hu, L. Su, L. Huang, Y. Liu, Z. Jin, A.A. Purezky, D.B. Geohegan, K. W. Kim, Y. Zhang, L. Cao, Equally efficient interlayer exciton relaxation and improved absorption in epitaxial and nonepitaxial MoS2/WS2 heterostructures, Nano Lett. 15 (2015) 486–491, https://doi.org/10.1021/nl5038177.
[23] S. Zhang, T.H. Nguyen, W. Zhang, Y. Park, W. Yang, Correlation between lateral size and gas sensing performance of MoSe2 nanosheets, Appl. Phys. Lett. 111 (2017), https://doi.org/10.1063/1.4986781.
[24] C. Casiraghi, A. Hartschuh, E. Lidorikis, H. Qian, H. Harutyunyan, T. Gokus, K. S. Novoselov, A.C. Ferrari, Rayleigh imaging of graphene and graphene layers, Nano Lett. 7 (2007) 2711–2717, https://doi.org/10.1021/nl071168m.
[25] S.V. Morozov, K.S. Novoselov, M.I. Katsnelson, F. Schedin, D.C. Elias, J. A. Jaszczak, A.K. Geim, Giant intrinsic carrier mobilities in graphene and its bilayer, Phys. Rev. Lett. 100 (2008) 11–14, https://doi.org/10.1103/PhysRevLett.100.016602.
[26] J. Wang, J. Song, X. Mu, M. Sun, Optoelectronic and photoelectric properties and applications of graphene-based nanostructures, Mater. Today Phys. 13 (2020), https://doi.org/10.1016/j.mtphys.2020.100196.
[27] D. Fadil, J. Sharma, M.I. Rizu, E. Llobet, Direct or indirect sonication in ecofriendly MoS 2 dispersion for NO 2 and NH 3 gas-sensing applications. https://doi.org/10.1021/acsomega.4c03166, 2024.
[28] V. Nicolosi, M. Chhowalla, M.G. Kanatzidis, M.S. Strano, J.N. Coleman, Liquid exfoliation of layered materials, Science 340 (2013) 72–75, https://doi.org/10.1126/science.1226419.
[29] K.A. Messalea, A. Zavabeti, M. Mohiuddin, N. Syed, A. Jannat, P. Atkin, T. Ahmed, S. Walia, C.F. McConville, K. Kalantar-Zadeh, N. Mahmood, K. Khoshmanesh, T. Daeneke, Two-Step synthesis of large-area 2D Bi2S3 nanosheets featuring high In-Plane anisotropy, Adv. Mater. Interfaces 7 (2020) 1–8, https://doi.org/10.1002/admi.202001131.
[30] Y. Hernandez, V. Nicolosi, M. Lotya, F.M. Blighe, Z. Sun, S. De, I.T. McGovern, B. Holland, M. Byrne, Y.K. Gun'ko, J.J. Boland, P. Niraj, G. Duesberg, S. Krishnamurthy, R. Goodhue, J. Hutchison, V. Scardaci, A.C. Ferrari, J. N. Coleman, High-yield production of graphene by liquid-phase exfoliation of graphite, Nat. Nanotechnol. 3 (2008) 563–568, https://doi.org/10.1038/nnano.2008.215.
[31] D. Fadil, R.F. Hossain, G.A. Saenz, A.B. Kaul, On the chemically-assisted excitonic enhancement in environmentally-friendly solution dispersions of two-dimensional MoS2 and WS2, J. Mater. Chem. C 5 (2017) 5323–5333, https://doi.org/10.1039/c7tc01001j.
[32] L. Zhang, Z. Li, J. Liu, Z. Peng, J. Zhou, H. Zhang, Y. Li, Optoelectronic gas sensor based on few-layered InSe nanosheets for NO2detection with ultrahigh antihumidity ability, Anal. Chem. 92 (2020) 11277–11287, https://doi.org/10.1021/acs.analchem.0c01941.
[33] L. Zhang, Q. Hao, J. Liu, J. Zhou, W. Zhang, Y. Li, Rolling up of 2D nanosheets into 1D Nanoscrolls: Visible-Light-activated chemiresistors based on surface modified indium selenide with enhanced sensitivity and stability, Chem. Eng. J. 446 (2022) 136937, https://doi.org/10.1016/j.cej.2022.136937.
[34] J. Le Fan, X.F. Hu, W.W. Qin, Z.Y. Liu, Y.S. Liu, S.J. Gao, L.P. Tan, J.L. Yang, L. B. Luo, W. Zhang, UV-light-assisted gas sensor based on PdSe2/InSe heterojunction for ppb-level NO2 sensing at room temperature, Nanoscale 14 (2022), https://doi.org/10.1039/d2nr03881a.
[35] W. Zheng, C. Yang, Z. Li, J. Xie, C. Lou, G. Lei, X. Liu, J. Zhang, Indium selenide nanosheets for photoelectrical NO2 sensor with ultra sensitivity and full recovery at room temperature, Sensors Actuators, B Chem. 329 (2021), https://doi.org/10.1016/j.snb.2020.129127.
[36] J. Sharma, F. Güell, M.I. Rizu, D. Fadil, E. Llobet, Highly selective hybrid InSe-Graphene for NO2 gas sensing with high humidity tolerance, ACS Sens. (2025), https://doi.org/10.1021/acssensors.4c03521.
[37] Z. Li, H. Qiao, Z. Guo, X. Ren, Z. Huang, X. Qi, S.C. Dhanabalan, J.S. Ponraj, D. Zhang, J. Li, J. Zhao, J. Zhong, H. Zhang, High-Performance photo-electrochemical photodetector based on liquid-exfoliated few-layered InSe nanosheets with enhanced stability, Adv. Funct. Mater. 28 (2018) 1–7, https://doi.org/10.1002/adfm.201705237.
[38] point group. At I' one has:, 25 (1978) 5-8.
[39] S.V. Sorokin, P.S. Avdienko, I.V. Sedova, D.A. Kirilenko, V.Y. Davydov, O. S. Komkov, D.D. Firsov, S.V. Ivanov, Molecular beam epitaxy of layered group III metal chalcogenides on GaAs(001) substrates, Materials 13 (2020), https://doi.org/10.3390/MA13163447.
[40] K. Krishnamoorthy, M. Veerapandian, G.-S. Kim, S. Jae Kim, A one step hydrothermal approach for the improved synthesis of graphene Nanosheets, Curr. Nanosci. 8 (2012) 934–938, https://doi.org/10.2174/157341312803989088.
[41] T. Wissink, M.C. Figueiredo, E.J.M. Hensen, Supplementary Information Stability of in 2 O 3 Nanoparticles PTFE-containing Gas Diffusion Electrodes for CO 2 Electroreduction to Formate, 67, 2023.
[42] S. Kumar, A. Garg, A. Chowdhuri, Sonication effect on graphene oxide (GO) membranes for water purification applications, Mater. Res. Express 6 (2019), https://doi.org/10.1088/2053-1591/ab1ffd.
[43] S. Ye, J. Feng, The effect of sonication treatment of graphene oxide on the mechanical properties of the assembled films, RSC Adv. 6 (2016), https://doi.org/10.1039/c6ra03996k.
[44] J. Lauth, F.E.S. Gorris, M. Samadi Khoshkhoo, T. Chassé, W. Friedrich, V. Lebedeva, A. Meyer, C. Klinke, A. Kornowski, M. Scheele, H. Weller, Solution-processed two-dimensional ultrathin InSe nanosheets, Chem. Mater. 28 (2016) 1728–1736, https://doi.org/10.1021/acs.chemmater.5b04646.
[45] M.C. Biesinger, Accessing the robustness of adventitious carbon for charge referencing (correction) purposes in XPS analysis: insights from a multi-user facility data review, Appl. Surf. Sci. 597 (2022), https://doi.org/10.1016/j.apsusc.2022.153681.
[46] Thermo Fisher Scientific, Oxygen X-ray photoelectron spectra, oxygen electron configuration, and other elemental information, Thermo Fish. Sci. 1 (2022). https://www.thermofisher.com/co/en/home/materials-science/learning-center/periodic-table/non-metal/oxygen.html.
[47] A. Chanthaphan, T. Hosoi, T. Shimura, H. Watanabe, Study of SiO2/4H-SiC interface nitridation by post-oxidation annealing in pure nitrogen gas, AIP Adv. 5 (2015), https://doi.org/10.1063/1.4930980.
[48] X. Chen, J. Hu, P. Chen, M. Yin, F. Meng, Y. Zhang, UV-light-assisted NO2 gas sensor based on WS2/PbS heterostructures with full recoverability and reliable anti-humidity ability, Sensors Actuators, B Chem. 339 (2021) 129902, https://doi.org/10.1016/j.snb.2021.129902.
[49] T.-C. Chen, Y.-C. Yang, H.-L. Liu, C.-M. Yang, M. Meyyappan, C.-S. Lai, in: The Effect of Monolayer Graphene on the UV Assisted NO2 Sensing and Recovery at Room Temperature, vol. 461, 2017, https://doi.org/10.3390/proceedings1040461.
[50] C.M. Yang, T.C. Chen, Y.C. Yang, M. Meyyappan, Annealing effect on UV-illuminated recovery in gas response of graphene-based NO2 sensors, RSC Adv. 9 (2019) 23343–23351, https://doi.org/10.1039/c9ra01295h.
[51] C. Lee, J. Kim, S. Kim, Y.J. Chang, K.S. Kim, B. Hong, E.J. Choi, Strong hole-doping and robust resistance-decrease in proton-irradiated graphene, Sci. Rep. 6 (2016) 1–9, https://doi.org/10.1038/srep21311.
[52] P.K. Sahu, R.K. Pandey, R. Dwivedi, V.N. Mishra, R. Prakash, Polymer/Graphene oxide nanocomposite thin film for NO2 sensor: an in situ investigation of electronic, morphological, structural, and spectroscopic properties, Sci. Rep. 10 (2020) 1–13, https://doi.org/10.1038/s41598-020-59726-5.
[53] J. Wu, Z. Wu, H. Ding, Y. Wei, W. Huang, X. Yang, Z. Li, L. Qiu, X. Wang, Flexible, 3D SnS2/Reduced graphene oxide heterostructured NO2 sensor, Sensors Actuators, B Chem. 305 (2020) 127445, https://doi.org/10.1016/j.snb.2019.127445.
[54] F. Yavari, E. Castillo, H. Gullapalli, P.M. Ajayan, N. Koratkar, High sensitivity detection of NO 2 and NH 3 in air using chemical vapor deposition grown graphene, Appl. Phys. Lett. 100 (2012), https://doi.org/10.1063/1.4720074.
[55] X. Yan, Y. Wu, R. Li, C. Shi, R. Moro, Y. Ma, L. Ma, High-Performance UV-Assisted NO2 sensor based on chemical vapor deposition graphene at room temperature, ACS Omega 4 (2019) 14179–14187, https://doi.org/10.1021/acsomega.9b00935.
[56] Y. Cai, G. Zhang, Y.W. Zhang, Charge transfer and functionalization of monolayer InSe by physisorption of small molecules for gas sensing, J. Phys. Chem. C 121 (2017) 10182–10193, https://doi.org/10.1021/acs.jpcc.7b02286.
[57] D. Ma, W. Ju, Y. Tang, Y. Chen, First-principles study of the small molecule adsorption on the InSe monolayer, Appl. Surf. Sci. 426 (2017) 244–252, https://doi.org/10.1016/j.apsusc.2017.07.198.
[58] N. Harathi, M. Bollu, K.S. Pasupuleti, Z. Tauanov, K.R. Peta, M.D. Kim, M. Reddeppa, A. Sarkar, V.N. Rao, PrGO decorated TiO2 nanoplates hybrid nanocomposite for augmented NO2 gas detection with faster gas kinetics under UV light irradiation, Sensors Actuators B Chem. 358 (2022) 131503, https://doi.org/10.1016/j.snb.2022.131503.
[59] L. Zhang, J. Zhang, Y. Huang, H. Xu, X. Zhang, H. Lu, K. Xu, P.K. Chu, F. Ma, Hexagonal ZnO nanoplates/graphene composites with excellent sensing performance to NO2 at room temperature, Appl. Surf. Sci. 537 (2021) 147785, https://doi.org/10.1016/j.apsusc.2020.147785.
[60] J. Bao, S. Zeng, J. Dai, X. Wang, Q. Liu, H. Li, X. Huang, W. Huang, Heterostructures between a tin-based intermetallic compound and a layered semiconductor for gas sensing, Chem. Commun. 57 (2021) 5590–5593, https://doi.org/10.1039/d1cc00015b.
[61] M. Reddeppa, B.G. Park, G. Murali, S.H. Choi, N.D. Chinh, D. Kim, W. Yang, M. D. Kim, NOx gas sensors based on layer-transferred n-MoS2/p-GaN heterojunction at room temperature: study of UV light illuminations and humidity, Sensors Actuators, B Chem. 308 (2020) 127700, https://doi.org/10.1016/j.snb.2020.127700.
[62] X. Duan, W. Zhao, R. Yan, T. Yu, W. Quan, Y. Chen, D. Xu, Efficient detection of NO2 in Rh-modified SnS/WS2 gas sensor: structural optimization and sensing performance improvement, Chem. Eng. J. 509 (2025), https://doi.org/10.1016/j.cej.2025.161219.
[63] Y. Cheng, Z. Li, T. Tang, X. Wang, X. Hu, K. Xu, M. Hung, N. Duc, H. Xie, H. Yu, H. Chen, J. Zhen, Journal of Colloid and Interface Science Functionalization :

towards high-performance room-temperature NO 2 Sensing, vol. 645, 2023, pp. 86–95.
[64] M. Kim, D. Yeom, Y. Seok, J. Song, H. Jang, Y. Choi, Y. Ko, K. Watanabe, T. Taniguchi, K. Lee, Minsu Kim, + Dongju Yeom, + Yongwook Seok, + Jungi Song, Hanbyeol Jang, YiTaek Choi, Yeonghyeon Ko, Kenji Watanabe, Takashi Taniguchi, and Kayoung Lee *, (2024).
[65] A. Bag, N.E. Lee, Gas sensing with heterostructures based on two-dimensional nanostructured materials: a review, J. Mater. Chem. C 7 (2019) 13367–13383, https://doi.org/10.1039/c9tc04132j.
[66] G. Jiménez-Cadena, J. Riu, F.X. Rius, Gas sensors based on nanostructured materials, Analyst 132 (2007) 1083–1099, https://doi.org/10.1039/b704562j.
[67] S. Kumar, A. Garg, A. Chowdhuri, Sonication effect on graphene oxide (GO) membranes for water purification applications, Mater. Res. Express 6 (2019) 85620, https://doi.org/10.1088/2053-1591/ab1ffd.
[68] B. Zhang, T. Chen, L. Wang, B. Yang, Study on ultrasonic dispersion of graphene nanoplatelets, Gongneng Cailiao/Journal Funct. Mater. 50 (2019) 8133–8139, https://doi.org/10.3969/j.issn.1001-9731.2019.08.019.
[69] O. Leenaerts, B. Partoens, F.M. Peeters, Adsorption of H2 O, N H3, CO, N O2, and NO on graphene: a first-principles study, Phys. Rev. B - Condens. Matter Mater. Phys. 77 (2008) 1–6, https://doi.org/10.1103/PhysRevB.77.125416.
[70] L.W. Bruch, M.W. Cole, H.Y. Kim, Transitions of gases physisorbed on graphene, J. Phys. Condens. Matter 22 (2010), https://doi.org/10.1088/0953-8984/22/30/304001.
[71] F. Schedin, A.K. Geim, S.V. Morozov, E.W. Hill, P. Blake, M.I. Katsnelson, K. S. Novoselov, Detection of individual gas molecules adsorbed on graphene, Nat. Mater. 6 (2007) 652–655, https://doi.org/10.1038/nmat1967.
[72] T.O. Wehling, M.I. Katsnelson, A.I. Lichtenstein, Adsorbates on graphene: impurity states and electron scattering, Chem. Phys. Lett. 476 (2009) 125–134, https://doi.org/10.1016/J.cplett.2009.06.005.
[73] Y. Zhou, C. Zou, X. Lin, Y. Guo, UV light activated NO2 gas sensing based on Au nanoparticles decorated few-layer MoS2 thin film at room temperature, Appl. Phys. Lett. 113 (2018) 2–7, https://doi.org/10.1063/1.5042061.